ASSESSING THE PERFORMANCE OF ECO-RETROFITTED SEAWALLS IN MITIGATING WAVE OVERTOPPING DISCHARGE – A NUMERICAL MODELLING STUDY

Xihang Xu[1], Jennifer Keenahan[2], M. A. Habib[1], Hanxiao Ma[1,3] and M. Salauddin[1*]

The enhancement of coastal resilience has become a key focus in sustainable development efforts. By increasing the topographic complexity of existing sea defences, eco-engineering interventions have been regarded as a potential approach for coastal biodiversity restoration and enhancement. However, only limited knowledge is available on the influences of these eco-retrofits on wave overtopping behaviour, such as the spatial distribution of the overtopping waves. The spatial distribution of wave overtopping is one of the critical indicators for determining the safe zone behind the coastal infrastructures. Therefore, this study contributes to the first parameter analysis on the influences of eco-retrofit geometrical characteristics on the spatial distribution of wave overtopping behind the eco-retrofitted seawall by conducting 32 numeric models in the scale of 1:10 through OpenFOAM®. A series of reference models are first established and validated with the experimental datasets. The validated models are then applied to study the influences of shape, width and length of eco-retrofits attached to the vertical seawall. It is found that even though the eco-retrofits have minimal influences on the largest travel distance of wave overtopping, a considerable impact on the spatial distribution of overtopping waves behind the structure was observed for the large structures. In general, a greater proportion of overtopping waves can travel greater distances when there is a larger structure length or width. For the small eco-retrofits, ignorable effects are observed both for the largest travel distance and the spatial distribution. The findings of this study provide a numerical dataset for designing eco-engineering interventions from an engineering perspective and indicate the effectiveness of OpenFOAM® in simulating and reproducing the wave-structure interactions.

Keywords: coastal resilience; eco-retrofitting structures; numerical modelling; OpenFOAM®; spatial distribution; wave overtopping; vertical seawall

INTRODUCTION

'Hard sea defences' or 'coastal armouring', such as seawalls and dikes, are conventionally employed by coastal engineers to safeguard coastal areas from flooding and erosion (Chen et al., 2021). Nevertheless, the smooth and featureless surfaces of these hard defenses result in lower structural complexity compared to natural coastal habitats, which can lead to a decrease in native biodiversity (Hall et al., 2019). Such destruction of biodiversity in nearby coastal regions and the inadequate response to climate change is increasingly driving improvements to traditional 'hard' sea defenses (Liu et al., 2022; Manousakas et al., 2022). Recognising this, in recent years, the terms including 'eco-engineering', 'hard eco-engineering', 'eco-retrofits' and 'eco-retrofitting interventions' have been spotlighted to describe the ecological interventions of existing 'hard' sea defences to restore and enhance the local habitats by improving the topographic complexity (O'Sullivan et al., 2020; Singhvi et al., 2022). To date, a considerable number of studies have demonstrated the ecological benefits of eco-engineered solutions, including "textured concrete" or "textured surface" tiles, 'drilled holes', 'vertipools', 'flowerpots' and 'living seawalls panels' (Evans et al., 2015). Nevertheless, studies of the influences of these structures on wave overtopping, particularly the spatial distribution of wave overtopping describing the relationship between overtopping volume and the travel distance of the overtopping water behind the sea defence, which is a crucial parameter to evaluate the safety zone after coastal infrastructures, are still very limited (Salauddin et al., 2022).

Based on the datasets from experiments and field measurements (Bruce et al., 2005; Pullen et al., 2006), Pullen et al. (2009) proposed an empirical relationship equation to describe and predict the spatial distribution of overtopping behind the vertical seawall as follows:

$$q^* = \frac{D'}{q_{total}} = e^{\left(-k(D')\right)} \tag{1}$$

in which, q^* represents the ratio of overtopping discharge lands after the normalised overtopping distance D' to the total discharge ($q_{D'}/q_{total}$), D' is defined as $D' = D/L$. k is the empirical coefficient that controls the shape of the

[1]UCD Dooge Centre for Water Resources Research, School of Civil Engineering, and UCD Earth Institute, University College Dublin, Dublin 4, Ireland.
[2]UCD School of Civil Engineering and UCD Earth Institute, University College Dublin, D04 V1W8 Dublin, Ireland.
[3]Chang'an Dublin International College of Transportation, Chang'an University, Xi'an, Shaanxi, China.
*Corresponding Author: md.salauddin@ucd.ie

spatial distribution of overtopping water behind the seawall, which is set as 29 when considering the significant sloping foreshore and ignoring the wind effects. Fig. 1 illustrates the main parameters employed by Eq. 1.

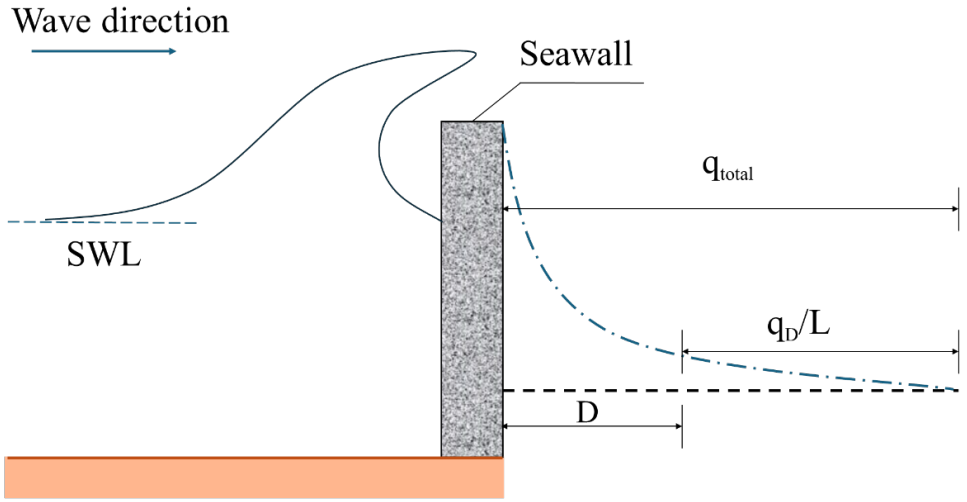

Figure 1. Schematic of parameters employed in describing and predicting the spatial distribution of wave overtopping: The q_D is the overtopping discharge in the distance of D behind the vertical seawall, q_{total} represents the total discharge of overtopping waves, L is the wavelength of the incident wave

In the past decade, OpenFOAM® has been widely adopted in reproducing wave overtopping behaviours in multiple sea defence structures, including dikes, breakwaters, and seawalls (Xu et al., 2024a; Higuera et al., 2013). However, while most studies focus on the simulation of total wave overtopping discharge on coastal defences, limited knowledge is available in the simulation and understanding of the spatial distribution of wave overtopping (Zhao et al., 2024). Therefore, this study aims to conduct a parameter analysis to evaluate the influences of geometrical characteristics (e.g., shape of cross-section, structure width and structure length) of a single eco-retrofit structure on the spatial distribution of wave overtopping behind the eco-retrofitted seawall by OpenFOAM® simulation.

LABORATORY SET-UP

Small-scale wave flume experiments measuring the spatial distribution of wave overtopping behind a vertical seawall with no influencing foreshore were performed at the Hydraulics Laboratory within the UCD School of Civil Engineering to validate the developed two-dimensional OpenFOAM model. Experiments were carried out in a wave flume (20 m long, 0.9 m wide and 0.6 m deep) equipped with a piston-type wave maker with an active wave absorption system (AWAS), enabling it to generate both regular and random wave patterns while minimizing the effects of wave reflection. Additionally, a mesh beach is available at the other end of the wave flume to absorb waves. The plain model seawall, which was 0.5 m deep, was constructed from a wooden board and positioned vertically at the centre of the wave flume, spanning the entire width of the channel. As shown in Fig. 2, the seawall was fixed 10.0 m away from the wave paddle during the experiments. To capture the characteristics of the incident wave conditions, including significant wave height and wave period, three wave gauges were placed near the wave paddle. adopting the 3-point approach.

To observe the spatial distribution of wave overtopping volumes, a multi-chamber container was constructed with wooden boards and attached to the model seawall. Fig. 3 shows the detailed design of the multi-chamber container. It is worth pointing out that a sharp-edge design on the top of each chamber's wall was made to reduce the overtopping jumping from one chamber to the adjacent chambers, as adopting the approach suggested by Dong et al (2020, 2021; 2024); Zhao et al (2024). The container was designed to have a higher resolution (smaller spacing between chambers) adjacent to the seawall, while the distance between each chamber increases when moving away from the seawall. The cumulative wave overtopping discharge measured in each chamber is therefore defined as the total discharge of wave

overtopping behind the seawall. The overtopping measurements in each chamber were continuously recorded in all the tests.

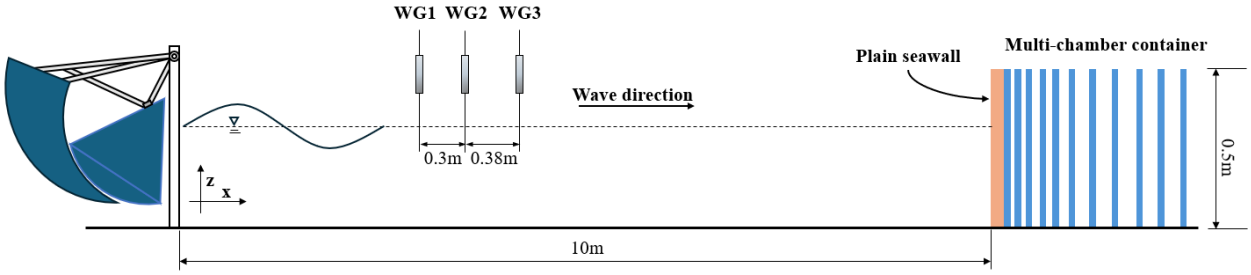

Figure 2. Schematic of 2D flume set-up and locations of wave gauges

Table 1 summarizes the incident regular wave conditions employed in this study, which all belong to Stokes II waves. Two wave steepness values, 0.015 and 0.05, were considered to simulate the swell and storm wave conditions. Two water depths (0.38 m and 0.42 m) corresponding to two freeboards of 0.12 and 0.08, respectively, were tested within this work.

Table 1. Summary of incident wave conditions for physical tests

Parameters	Values
Water depth *h* (m)	0.38, 0.42
Incident wave height *H* (m)	0.05, 0.06, 0.07, 0.08, 0.09
Incident wave period *T* (s)	0.8, 0.88, 0.95, 1.01, 0.46, 0.6, 1.73, 1.85, 1.96
Wavelength *L* (m)	1, 1.2, 1.4, 1.6, 3.33, 4, 4.67, 5.33
Wave steepness *S (H/L)*	0.015, 0.05

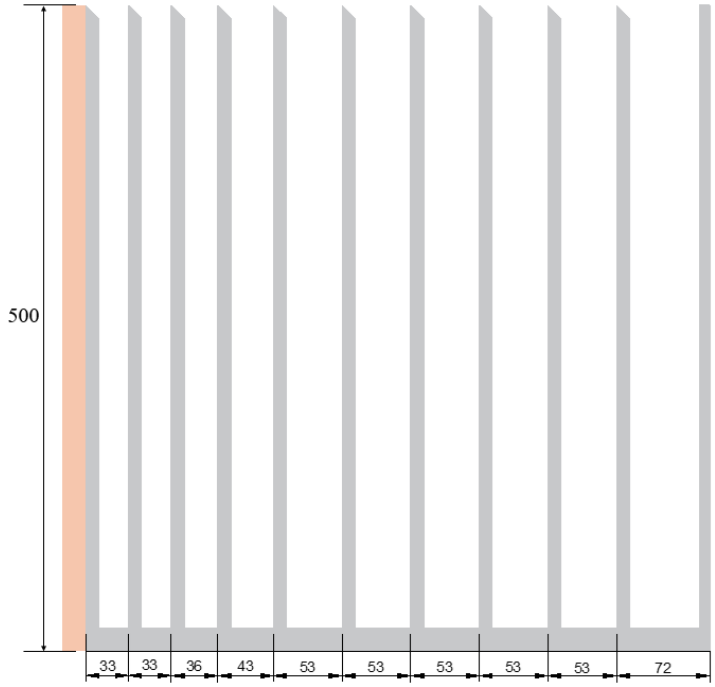

Figure 3. Design of a multi-chamber container for the spatial distribution measurements behind the plain seawall (in mm)

NUMERICAL SETUP

In this study, a two-dimensional numerical model was developed using an open-source Computational Fluid Dynamics (CFD) toolbox, OpenFOAM®, which has been proven to provide a strong performance in simulating wave-structure interactions (Xu et al., 2024b). The Reynolds Averaged Navier-Stokes (RANS) equations, including continuity and mass conservation equations (Eq. 2 and Eq. 3), for incompressible flows, were taken as the control equations for the numerical model, and the 'interIsoFoam' solver within OpenFOAM was adopted to solve RANS equations.

$$\nabla \cdot \mathbf{U} = \mathbf{0} \tag{2}$$

$$\frac{\partial \rho \mathbf{U}}{\partial t} + \nabla \cdot (\rho \mathbf{U}\mathbf{U}) - \nabla \cdot \left(\mu_{eff} \nabla \mathbf{U}\right) = -\nabla p^* - \mathbf{g} \cdot X \nabla \rho + \nabla \mathbf{U} \cdot \nabla \mu_{eff} + \sigma \kappa \nabla \alpha \tag{3}$$

where, $\mathbf{U}$ is the velocity vector; p^* is the pseudo-dynamic pressure; $\mathbf{g}$ represents gravity acceleration; μ_{eff} is the efficient dynamic viscosity; ρ is the density of the cell, which can be calculated using the volume of fluid (VOF) method.

In order to capture the sharp interface moving between two incompressible phases (air and water in this case), the isoAdvector interface advection algorithm based on the VOF method developed by Roenby et al (2016) was employed in this study by using the 'interIsoFoam' solver. The isoAdvector algorithm, suitable for arbitrary meshes, has been proven to save computational time while maintaining accurate geometrical resolution.

The numerical solution was obtained by the PIMPLE algorithm, which is a combination of PISO (pressure implicit with splitting of operators) and SIMPLE (semi-implicit method for pressure-linked equations) algorithms and allows equation under relaxation to keep the convergency of all equations in each time step. Even though $k-\varepsilon$ and $k-\omega\ SST$ turbulence model was found to be applied in previous wave-structure interaction analyses with the wave-breaking phenomenon; some studies also demonstrate a sufficient capacity for applying the laminar model in simulating wave-structure interactions and obtaining the adequate estimation of bulk hydrodynamic variables (Ravindar et al., 2022; Molines et al., 2020; Jacobsen et al., 2018). Therefore, this study is carried out considering incompressible water and air while ignoring the turbulence and a similar technique is employed. The developed numerical model is validated with the experimental dataset before starting the parameter analysis. The Courant number was limited to 0.5 to ensure the stability of the numerical model.

The 2D numerical wave flume was generated regarding the experimental setup, as shown in Fig. 4. Instead of the relaxation zone, an active wave absorption function was applied at the inlet boundary to generate and absorb waves while ensuring an acceptable calculation time. The front and back sides of the computational domain were set as empty to be excluded from the calculation. The outlet, seawall, multi-chamber container and flume bottom were set as no-slip wall boundaries. The upper boundary was set as inletAndoutlet boundary, where the air, water and pressure can leave the domain.

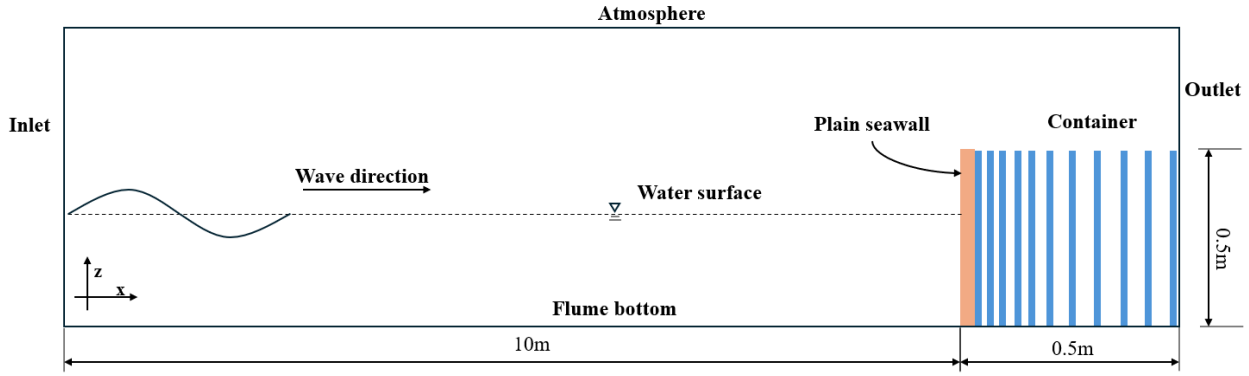

Figure 4. Schematic of the developed computational domain

The geometries of eco-retrofitted seawalls and multi-chamber containers were created by the third-party software BLENDER. The mesh generation tools, 'blockMesh' and 'snappyHexMesh', were then applied to generate the computational domain, as shown in Fig. 5. The mesh near the water surface was refined at the second refinement level, while the mesh in the model area was refined at the third level to capture the geometrical features accurately. It is known that the wave simulation performance is highly dependent on the mesh characteristics, more specifically, the cell size in the X direction (Δx) is related to wavelength (L) while the cell size in the Z direction (Δz) is related to wave height (H). The setting of 9 to 14 cells per wave height was found in previous studies (Zhao et al., 2024). To quantitively study the influences of mesh characteristics on the wave simulation performance, a mesh convergency study was conducted, as shown in Table 2.

Table 2. Mesh resolution of the free surface in this study

Mesh resolution (free surface)	Δx (m)	Δz (m)	Cells per wave height	Cells per wavelength
Mesh 1	0.01	0.01	5-9	80-196
Mesh 2	0.005	0.005	10-18	160-392
Mesh 3	0.0025	0.0025	20-36	320-784
Mesh 4	0.005	0.0025	10-18	320-784

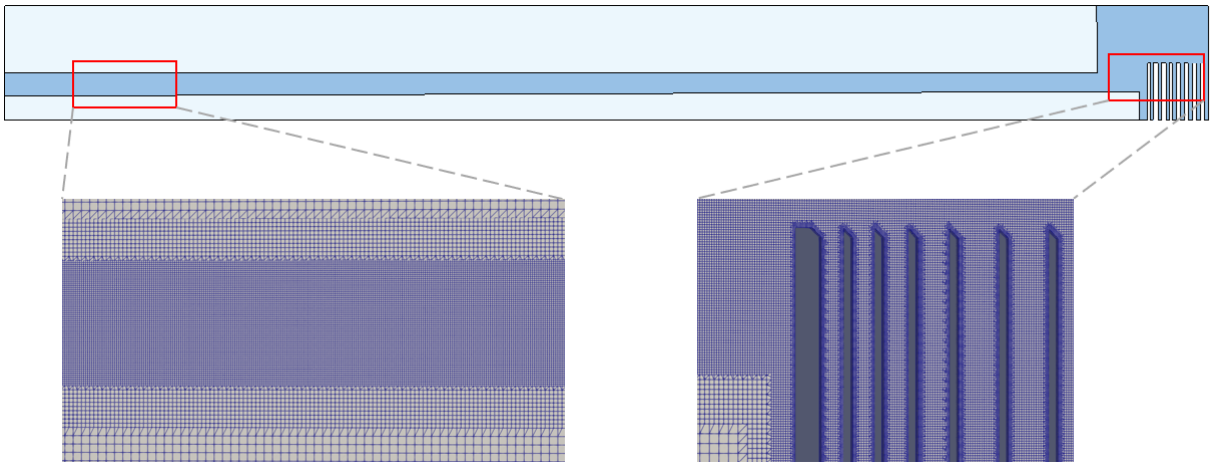

Figure 5. Mesh distribution and refinement of the numerical domain

To quantify the wave overtopping discharge in each chamber, a series of probes were placed inside the multi-chamber container at the same elevation as the previous study (Zhao et al., 2024). Each probe was placed directly at the centre of each cell, which makes it capable of recording the fluid flux (ϕ_F) and water fraction that passes through each cell at every time step. The instantaneous water flux over the selected faces S can be calculated as Eq. 4:

$$q = \sum_{f \in S} \varphi_{F,f} \frac{\mathbf{S}_f}{\mathbf{S}_{f,2}}, \varphi_F = \frac{\varphi_\rho - \rho_{F=0}\varphi}{\rho_{F=1} - \rho_{F=0}} \tag{4}$$

where $\mathbf{S}_f$ indicates the non-unit normal vector to the face. The cumulative overtopping volume (V) could then be estimated as the sum of overtopping volume per chamber, shown as Eq. 5:

$$V_{total} = \sum_{t=t_{start}}^{t_{end}} q\Delta t \tag{5}$$

in which, Δt is the write interval of each recording.

MODEL VALIDATION

In order to test and validate the capacity of the developed wave simulation and optimise the mesh configuration to save computational time while maintaining the modelling performance. A mesh convergency study was conducted first for several wave conditions. To quantify the reliability and accuracy of the developed model, the Root Mean Squared Error (RMSE) and Pearson correlation coefficient were employed as Eq. 6:

$$r = \frac{\sum_{i=1}^{n} (\eta_{theoretical} - \overline{\eta_{theoretical}})(\eta_{numerical} - \overline{\eta_{numerical}})}{\sqrt{\sum_{i=1}^{n} (\eta_{theoretical} - \overline{\eta_{theoretical}})^2}\sqrt{\sum_{i=1}^{n} (\eta_{numerical} - \overline{\eta_{numerical}})^2}} \tag{6}$$

Fig. 6 demonstrates the comparison between numerical and Stokes II theoretical water surface elevation variation without seawall for h=0.42m, H=0.07m and T=1.73s. Table 3 summarises the calculated RMSE and Pearson correlation coefficient of each mesh configuration. It can be found that even though the developed model slightly overpredicts the wave troughs, the overall quality of the simulated wave profile fits well with theoretical data and only minimal wave height attenuation was observed, which may be caused by the water viscosity effects. All these four mesh resolutions have a good capacity for wave generation and propagation, and the finer mesh contributes to more accurate simulation. However, it is worth pointing out that the aspect ratio of the cell is recommended to be set as 1 ($\Delta x = \Delta y$), which fits the theoretical data best as the previous study. Therefore, mesh 3 is adopted for the later validation. Fig. 7 shows the comparison between numerical and Stokes II theoretical water surface elevation without seawall for h=0.42, H=0.08m and T=1.85s, H=0.06m and T=0.88s, h=0.38m. H=0.08m and T=1.85s. Even though the increase in wave steepness slightly decreases the performance of the numerical model, the modelled water surface profile fits Stokes II wave theory well.

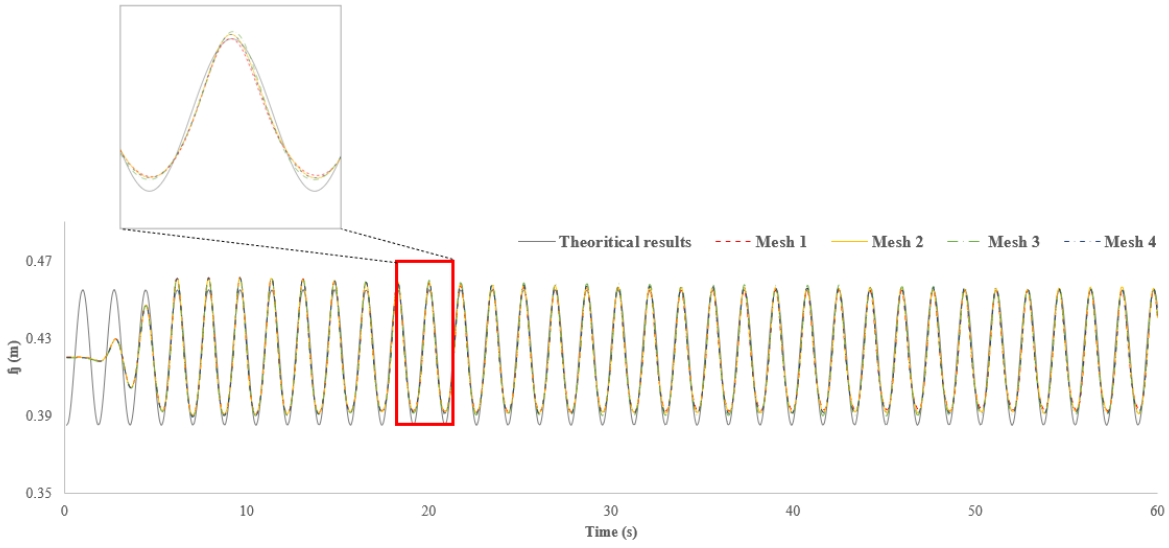

Figure 6. Comparison of numerical and theoretical water surface at 2.6m from wave paddle of four mesh configurations (h=0.42m, H=0.07m, T=1.73s)

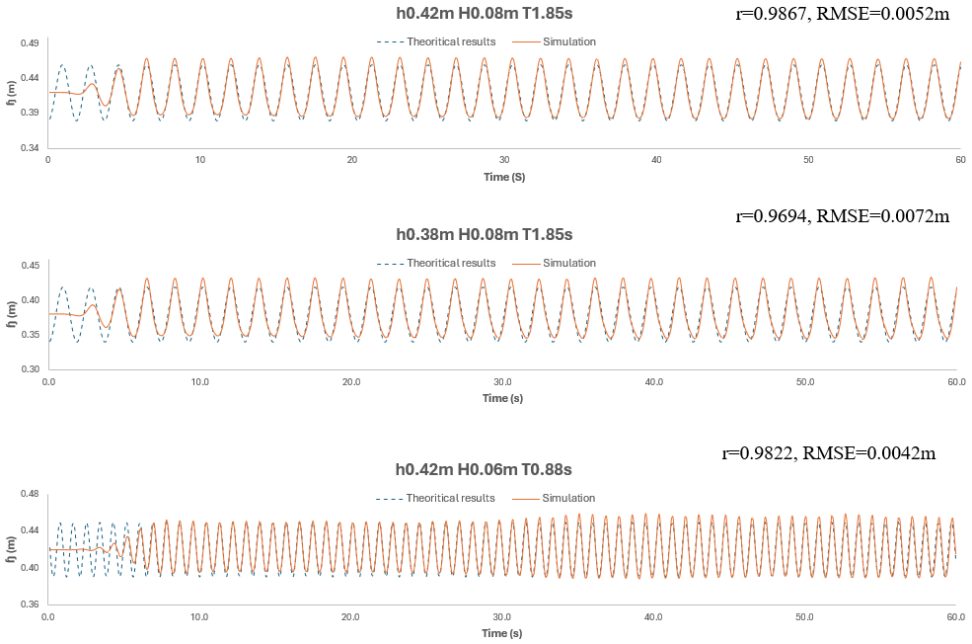

Figure 7. Comparison between numerical and theoretical water elevation variation without seawall

Table 3. The RMSE and Pearson correlation coefficient for each model

Mesh resolution	Pearson correlation coefficients (r)	RMSE
Mesh 1	0.98600	0.0046m
Mesh 2	0.98860	0.0040m
Mesh 3	0.98955	0.0037m
Mesh 4	0.98805	0.0041m

The comparison in this section proves the capacity of OpenFOAM to accurately simulate the regular wave generation and wave propagation over the flat flume bottom. Based on the consideration of modelling performance and computational time, mesh three resolution is therefore employed for further research, and Table 4 provides the mesh size for different regions in the computational domain.

Table 4. Employed mesh resolution for different regions in the computational domain

Mesh region	Δx (m)	Δz (m)
Background mesh	0.01	0.01
Free surface mesh	0.0025	0.0025
Mesh near the geometries	0.00125	0.00125

Furthermore, the spatial distribution of wave overtopping behind the plain vertical seawall was validated by comparing the numerical results with experimental datasets. Four multi-chamber container arrangements were considered: without multi-chamber container, experimental multi-chamber setting, experimental multi-chamber arrangement with 0.01m chamber wall, and experimental multi-chamber arrangement with 0.005m chamber wall. Consistent with the previous study (Zhao et al., 2024), the multi-chamber container's arrangement will influence the numerical model's performance in predicting the spatial distribution of wave overtopping, which may be because of the numerical dissipation. Fig. 8 demonstrates a considerable bias between modelling and experimental results when applying the same arrangement with experimental settings. The inconsistency of numerical results without the multi-chamber container and experimental data was observed. Zhao et al. (2024) explained that the collection of water volume is highly affected by the motion and propagation of waves. When there is no container, the fast propagation of water leads to errors in the collection. The reduction in chamber wall thickness can significantly enhance the

performance of the developed model, which shows an opposite trend to the previous study (Zhao et al., 2024). This might be due to the different settings of geometries and wave conditions. Both 0.005m and 0.01m chamber wall thickness led to a good convergence with the experimental dataset without significant differences in computational time. The RMSE values are 0.0131 and 0.0173, respectively. Therefore, the experimental multi-chamber container arrangement with 0.005m wall thickness is adopted for further study.

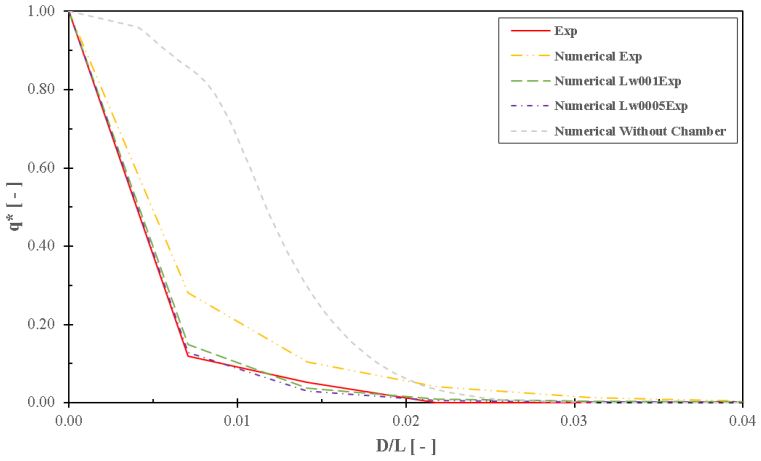

Figure 8. Comparison between numerical results and experimental data on the spatial distribution of wave overtopping ('Lw001 Exp' represents the same chamber arrangement with experimental settings with 0.01m chamber wall width while 'Lw0005 Exp' represents the experimental chamber setting with 0.005m chamber wall width)

PARAMETER SETTINGS OF ECO-RETROFITS

Fig. 9 illustrates the arrangement of multiple simplified eco-retrofits, including rectangular and triangular cross-sections, which represent the most common types of eco-engineering interventions that have been applied worldwide, such as 'flowerpots', 'vertipools', 'texture' and 'tiles', etc (Salauddin et al., 2021). In the real world, most eco-retrofitting structures are placed in the intertidal position; therefore, the eco-retrofit's centre is aligned with the water surface. It was found that the maximum distance from the seawall surface to the furthest position of eco-retrofits could be 40cm, while the maximum length of eco-retrofits (from top to tip) could be 61cm. Based on the assumptions of 1) the surface roughness won't play a significant role in influencing the spatial distribution of wave overtopping compared with structure geometries; 2) the hollow part within the eco-retrofits won't contribute to the influences, a geometrical scaling of 1 in 10 was therefore employed to design the scaled eco-retrofits, as summarised in Table 5. A matrix of 32 eco-retrofit configurations was undertaken for the intertidal position covering the smallest and largest sizes of eco-retrofits, as shown in Fig. 9. The wave conditions h=0.42m, H=0.07m and T=1.73s were applied to all 32 simulations.

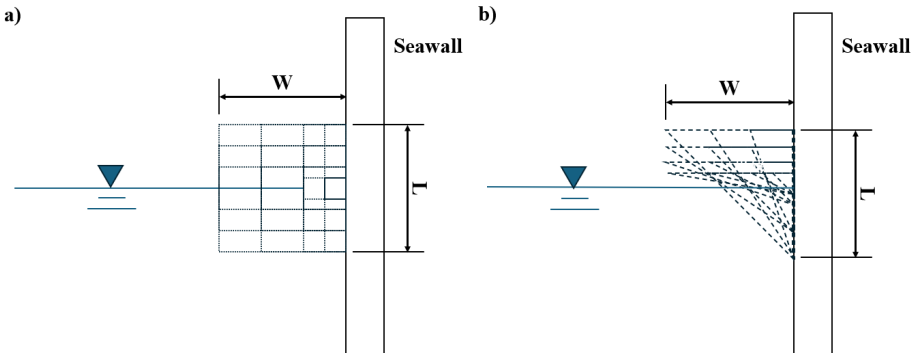

Figure 9. Schematic of multiple eco-retrofits with different dimensions: a) rectangular cross-section representing eco-retrofits such as 'flowerpots'; b) triangular cross-section representing eco-retrofits such as 'vertipools'. 'W' is the distance from the seawall to the furthest position of the structure, 'L' is the length of the structure (from top to tip)

Table 5. Summary of eco-retrofit configurations employed in this study

Simulation Ref.	Cross-section	Width *W* (cm)	Length *L* (cm)	Simulation Ref.	Cross-section	Width *W* (cm)	Length *L* (cm)
Case-w1l1	Rectangular	1	1	Case-tw1l1	Triangular	1	1
Case-w1l2		1	2	Case-tw1l2		1	2
Case-w1l4		1	4	Case-tw1l4		1	4
Case-w1l6		1	6	Case-tw1l6		1	6
Case-w2l1		2	1	Case-tw2l1		2	1
Case-w2l2		2	2	Case-tw2l2		2	2
Case-w2l4		2	4	Case-tw2l4		2	4
Case-w2l6		2	6	Case-tw2l6		2	6
Case-w4l1		4	1	Case-tw4l1		4	1
Case-w4l2		4	2	Case-tw4l2		4	2
Case-w4l4		4	4	Case-tw4l4		4	4
Case-w4l6		4	6	Case-tw4l6		4	6
Case-w6l1		6	1	Case-tw6l1		6	1
Case-w6l2		6	2	Case-tw6l2		6	2
Case-w6l4		6	4	Case-tw6l4		6	4
Case-w6l6		6	6	Case-tw6l6		6	6

RESULTS

Fig. 10 demonstrates the effect of structure length *L* of rectangular interventions on the spatial distribution of wave overtopping behind the eco-retrofitted seawall, where D represents the distance to the vertical seawall, and H represents the incident wave height (0.07m in this case). Even though the inconsistency of trends was observed in different width groups, generally, with the increase of structure length, fewer overtopping waves can pass to a farther distance. The minimal effect was observed when the structure width was only 1 or 2 cm, while this effect became more significant for larger structure widths. It is known that the travel distance of the overtopped wave depends on the velocity and layer thickness of the overtopping water (Schüttrumpf & Oumeraci, 2005). Therefore, the increase in structure length may reduce the velocity and layer thickness of the overtopping water. The higher structure width can strengthen this phenomenon. The increase in structure width *W* has a similar but stronger effect on the spatial distribution of wave overtopping than the structure length, especially for the relatively small geometry, as shown in

Fig. 11. However, this influence of structure width was decreased with the increase of structure length. Therefore, there might exist a threshold value of the geometrical size that structure width drives the influences of eco-retrofits in the spatial distribution of wave overtopping for the relatively small geometry (e.g., the width and length are equal or smaller than 2cm); in contrast, the influences are dominated by the structure length for the relatively large geometry (e.g., the width and length are larger than 2cm). However, further studies are required to determine this threshold value.

As for the eco-retrofits with a triangular cross-section, only limited influences on the spatial distribution were observed for the relatively small geometries consistent with the rectangular section study. When the structure width is smaller than 6cm, the increase in structure length leads to an ignorable influence on the spatial distribution. However, when the structure width is 6cm, which might be a critical value, the proportion of wave overtopping passing through a specific distance intends to increase with the increase of structure length, as shown in Fig. 12. When the structure length is smaller than 6cm, a negative correlation was found between the structure width and the proportion of water passing through a distance D. When the structure length is 6cm, however, the structure width only has an ignorable effect on the spatial distribution of wave overtopping as shown in Fig. 13.

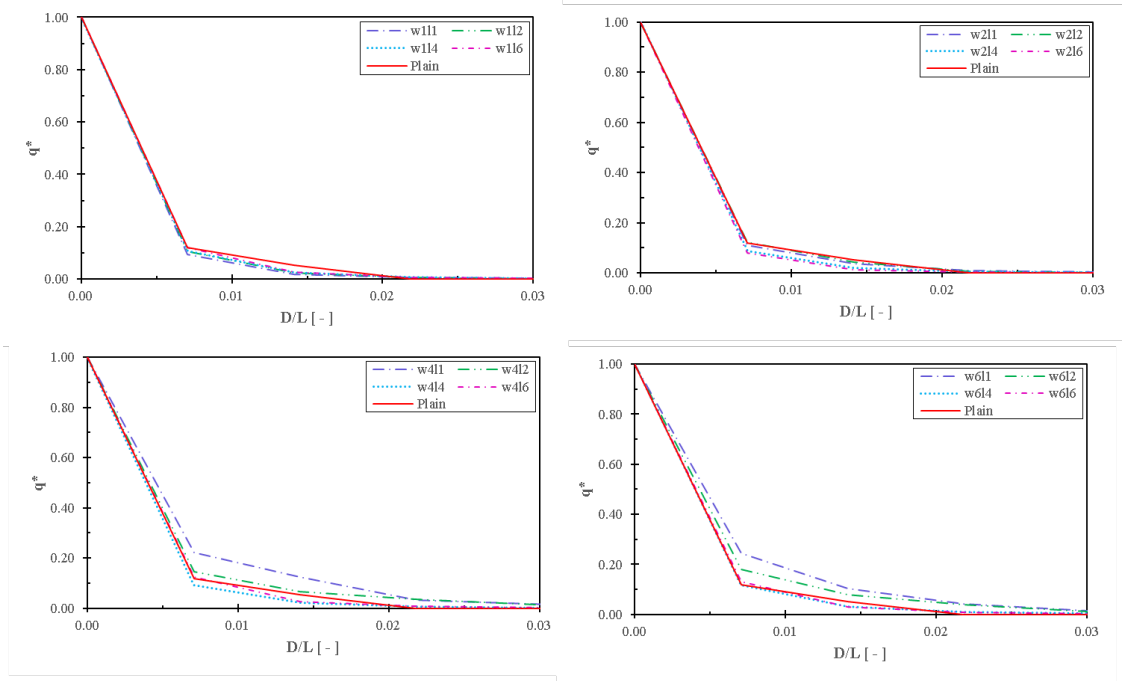

Figure 10. Influences of rectangular eco-retrofits' length on the spatial distribution of wave overtopping (w1l1 indicates 1cm width, 1cm length)

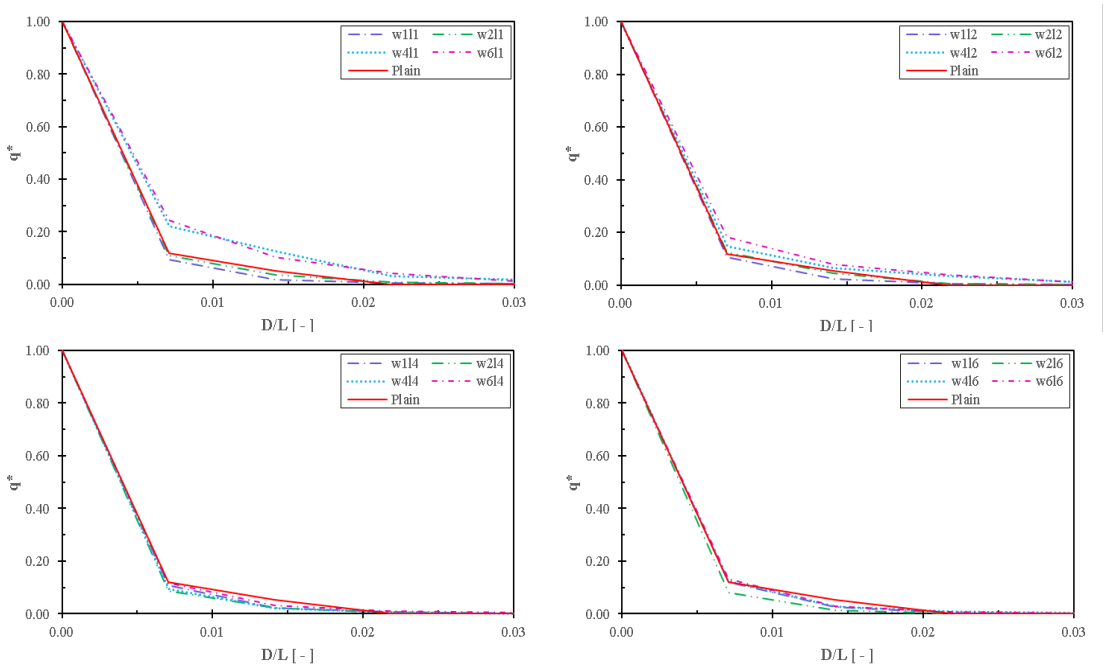

Figure 11. Influences of rectangular eco-retrofits' width on the spatial distribution of wave overtopping

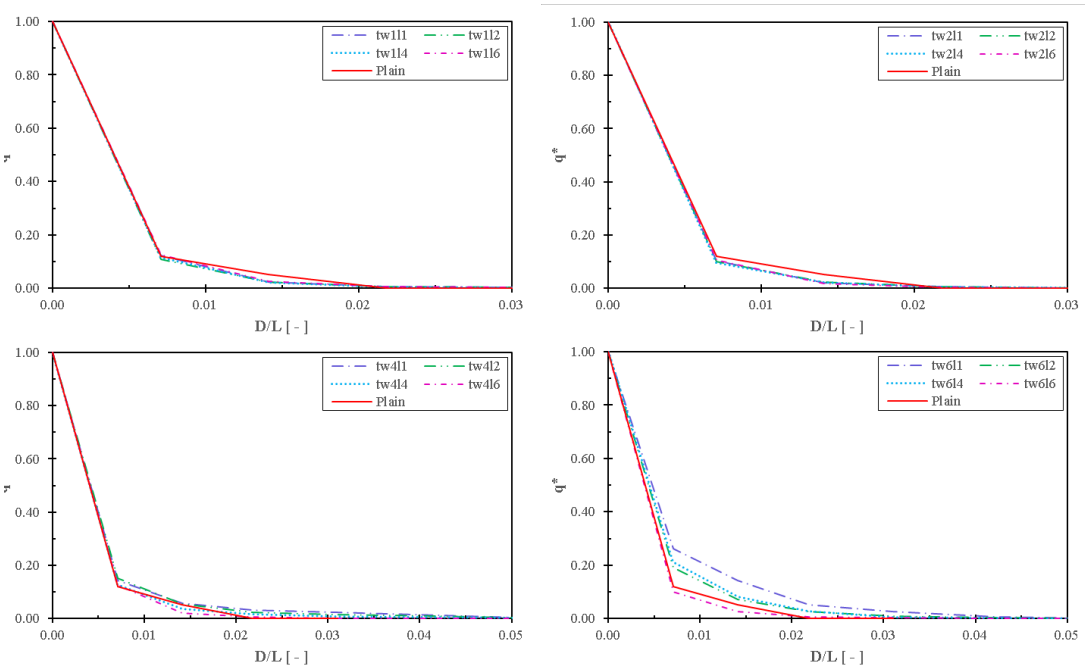

Figure 12. Influences of triangular eco-retrofits' length on the spatial distribution of wave overtopping (tw1l1 indicates triangular interventions with 1cm width, 1cm length)

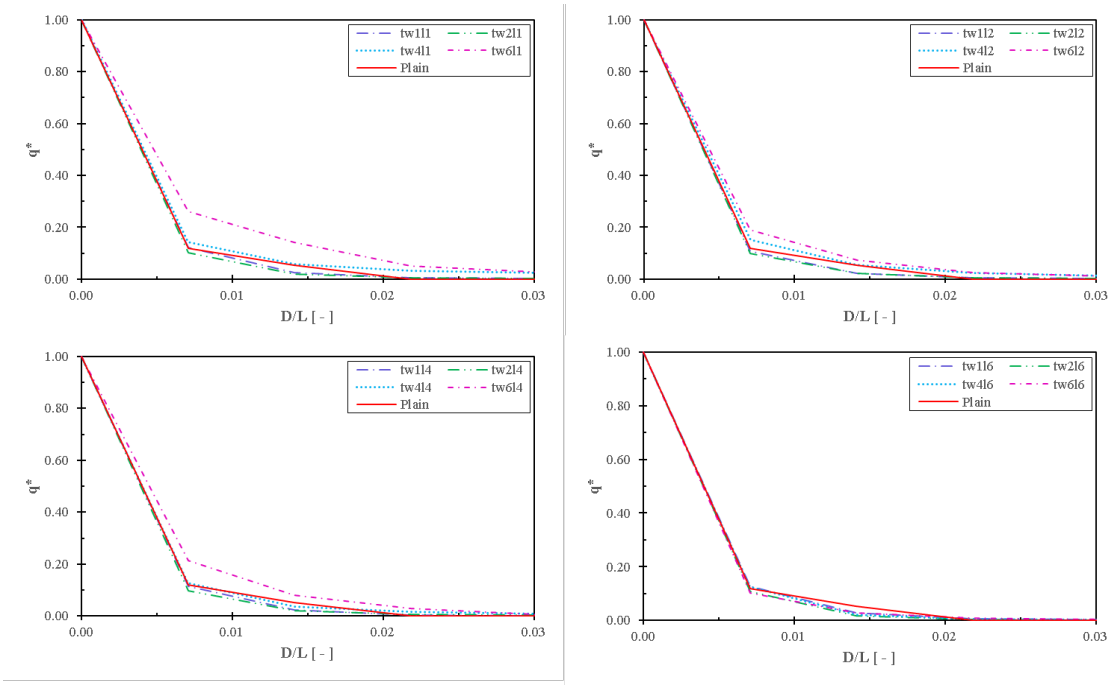

Figure 13. Influences of triangular eco-retrofits' width on the spatial distribution of wave overtopping

Overall, the influences of eco-engineering interventions on the spatial distribution of wave overtopping are found to be highly dependent on the geometrical characteristics. A minimum value of geometry size is required to activate the influences. The similar influence patterns were found for both rectangular and triangular cross-sections; for instance, regarding triangular cross-sections, structure width dominates the impact of relatively small eco-retrofits, while structure length drives the influences of relatively large eco-retrofits. The larger the structure width/length, the more percent of overtopping waves can travel to a relatively far distance. Additionally, it is worth pointing out that all 32 no. of eco-retrofit configurations have minimal impact on the maximum travel distance for the overtopping waves.

CONCLUSIONS

While much of the focus has been on the ecological benefits of eco-retrofitting and eco-engineering interventions, there is limited understanding of how these interventions impact the spatial distribution of wave overtopping behind eco-retrofitted seawalls. This paper presents results and analysis of a series of numerical simulations to observe the effects of various geometrical characteristics of eco-retrofitting (such as cross-sectional shape, width, and length) on wave overtopping distribution. The developed 2D numerical model was first validated through two ways: 1) by comparing the modelled variations in water surface elevation with theoretical data from Stokes II waves, and 2) by comparing the modelled spatial distribution of wave overtopping behind a plain vertical seawall with experimental data. The validated model was subsequently applied for the analysis of spatial overtopping parameters. The results of this study showed that tested eco-retrofit configurations have minimal effects on the largest travel distance of the overtopping wave. Additionally, the cross-sectional shape of eco-retrofits exerts negligible influences of eco-retrofitting interventions on the spatial distribution of wave overtopping in most cases. Nonetheless, the findings also indicate that the scale of eco-retrofits substantially influences the impact patterns of its geometrical features on the spatial distribution of wave overtopping. In this study, numerical simulations were conducted solely under regular wave conditions. Future research should investigate the spatial distribution of wave overtopping at eco-retrofitted solutions under irregular and extreme wave conditions. Additionally, it would be beneficial to examine how the placement techniques of eco-retrofits affect their performance, while also considering the roughness and porosity of these interventions.

ACKNOWLEDGEMENTS

Xihang Xu gratefully acknowledges the financial support from the University College Dublin and the China Scholarship Council. The numerical modelling was carried out under the support of the Irish Centre for High-End Computing (ICHEC) and the UCD Sonic High-Performance Computing (HPC) cluster.

REFERENCES

Bruce, T., Pullen, T., Allsop, W., & Pearson, J. 2005. How far back from a seawall is safe? Spatial distributions of wave overtopping. In *International Conference on Coastlines, structures and breakwaters 2005* (pp. 166–175). Thomas Telford Publishing. https://doi.org/10.1680/csab2005hsad.34556.0015

Chen, L. F., Zang, J., Hillis, A. J., Morgan, G. C. J., & Plummer, A. R. 2014. Numerical investigation of wave–structure interaction using OpenFOAM. *Ocean Engineering*, *88*, 91–109. https://doi.org/10.1016/j.oceaneng.2014.06.003

Dong, S., Abolfathi, S., Salauddin, M., & Pearson, J. 2020. Spatial distribution of wave-by-wave overtopping at vertical seawalls. *Coastal Engineering Proceedings*, *36v*, Article 36v. https://doi.org/10.9753/icce.v36v.structures.17

Dong, S., Abolfathi, S., Salauddin, M., & Pearson, J. M. 2021. Spatial distribution of wave-by-wave overtopping behind vertical seawall with recurve retrofitting. *Ocean Engineering*, *238*, 109674. https://doi.org/10.1016/j.oceaneng.2021.109674

Dong, S., Salauddin, M., Abolfathi, S., & Pearson, J. M. 2024. Improved prediction of wave overtopping rates at vertical seawalls with recurve retrofitting. *Ocean Engineering*, *302*, 117647. https://doi.org/10.1016/j.oceaneng.2024.117647

Evans, A. J., Firth, L. B., Hawkins, S. J., Morris, E. S., Goudge, H., Moore, P. J., Evans, A. J., Firth, L. B., Hawkins, S. J., Morris, E. S., Goudge, H., & Moore, P. J. 2015. Drill-cored rock pools: An effective method of ecological enhancement on artificial structures. *Marine and Freshwater Research*, *67*(1), 123–130. https://doi.org/10.1071/MF14244

Hall, A. E., Herbert, R. J. H., Britton, J. R., Boyd, I. M., & George, N. C. 2019. Shelving the Coast With Vertipools: Retrofitting Artificial Rock Pools on Coastal Structures as Mitigation for Coastal Squeeze. *Frontiers in Marine Science*, *6*. https://www.frontiersin.org/articles/10.3389/fmars.2019.00456

Higuera, P., Lara, J. L., & Losada, I. J. 2013. Realistic wave generation and active wave absorption for Navier–Stokes models: Application to OpenFOAM®. *Coastal Engineering*, *71*, 102–118. https://doi.org/10.1016/j.coastaleng.2012.07.002

Jacobsen, N. G., van Gent, M. R. A., Capel, A., & Borsboom, M. 2018. Numerical prediction of integrated wave loads on crest walls on top of rubble mound structures. *Coastal Engineering*, *142*, 110–124. https://doi.org/10.1016/j.coastaleng.2018.10.004

Larsen, B. E., Fuhrman, D. R., & Roenby, J. 2019. Performance of interFoam on the simulation of progressive waves. *Coastal Engineering Journal*. https://www.tandfonline.com/doi/abs/10.1080/21664250.2019.1609713

Liu, N., Salauddin, M., Yeganeh-Bakhtiari, A., Pearson, J., & Abolfathi, S. 2022. The Impact of Eco-retrofitting on Coastal Resilience Enhancement – A Physical Modelling Study. *IOP Conference Series: Earth and Environmental Science*, *1072*(1), 012005. https://doi.org/10.1088/1755-1315/1072/1/012005

Manousakas, N., Salauddin, M., Pearson, J., Denissenko, P., Williams, H., & Abolfathi, S. 2022. Effects of Seagrass Vegetation on Wave Runup Reduction – A Laboratory Study. *IOP Conference Series: Earth and Environmental Science*, *1072*(1), 012004. https://doi.org/10.1088/1755-1315/1072/1/012004

Molines, J., Bayón, A., Gómez-Martín, M. E., & Medina, J. R. 2020. Numerical Study of Wave Forces on Crown Walls of Mound Breakwaters with Parapets. *Journal of Marine Science and Engineering*, *8*(4), Article 4. https://doi.org/10.3390/jmse8040276

O'Sullivan, J., Salauddin, M., Abolfathi, S., & Pearson, J. 2020. Effectiveness of eco-retrofits in reducing wave overtopping on seawalls. *Coastal Engineering Proceedings*, *36v*, Article 36v. https://doi.org/10.9753/icce.v36v.structures.13

Pullen, T., Allsop, W., & Bruce, T. 2006. Wave overtopping at vertical seawalls: Field and laboratory measurements of spatial distributions. In *Coastal Engineering 2006* (pp. 4702–4713). World Scientific Publishing Company. https://doi.org/10.1142/9789812709554_0394

Pullen, T., Allsop, W., Bruce, T., & Pearson, J. 2009. Field and laboratory measurements of mean overtopping discharges and spatial distributions at vertical seawalls. *Coastal Engineering*, *56*(2), 121–140. https://doi.org/10.1016/j.coastaleng.2008.03.011

Ravindar, R., Sriram, V., & Salauddin, M. 2022. Numerical modelling of breaking wave impact loads on a vertical seawall retrofitted with different geometrical configurations of recurve parapets. *Journal of Water and Climate Change*, *13*(10), 3644–3674. https://doi.org/10.2166/wcc.2022.211

Roenby, J., Bredmose, H., & Jasak, H. 2016. A computational method for sharp interface advection. *Royal Society Open Science*, *3*(11), 160405. https://doi.org/10.1098/rsos.160405

Salauddin, M., O'Sullivan, J. J., Abolfathi, S., & Pearson, J. M. 2021. Eco-Engineering of Seawalls—An Opportunity for Enhanced Climate Resilience From Increased Topographic Complexity. *Frontiers in Marine Science*, *8*. https://www.frontiersin.org/articles/10.3389/fmars.2021.674630

Salauddin, M., O'Sullivan, J.J., Abolfathi, S., Peng, Z., Dong, S. and Pearson, J.M., 2022. New insights in the probability distributions of wave-by-wave overtopping volumes at vertical breakwaters, *Scientific Reports*, 12(1), p.16228. https://doi.org/10.1038/s41598-022-20464-5

Schüttrumpf, H., & Oumeraci, H. 2005. Layer thicknesses and velocities of wave overtopping flow at seadikes. *Coastal Engineering*, *52*(6), 473–495. https://doi.org/10.1016/j.coastaleng.2005.02.002

Singhvi, A., Luijendijk, A. P., & van Oudenhoven, A. P. E. (2022). The grey – green spectrum: A review of coastal protection interventions. *Journal of Environmental Management*, *311*, 114824. https://doi.org/10.1016/j.jenvman.2022.114824

Xu, X., Keenahan, J., & Salauddin, M. 2024a. Wave-Structure Interactions at Sea Defences Using Numerical Modelling Approaches: A Systematic Literature Review. In D.-S. Jeng & D. Wan (Eds.), *Proceedings of 10th International Conference on Coastal and Ocean Engineering* (pp. 3–17). Springer Nature. https://doi.org/10.1007/978-981-97-5353-6_1

Xu, X., Salauddin, M., & Keenahan, J. 2024b. A convergence study simulating regular waves using the k-ω SST turbulence model in OpenFOAM®. *IOP Conference Series: Materials Science and Engineering*, *1312*(1), 012006. https://doi.org/10.1088/1757-899X/1312/1/012006

Zhao, H., Ye, J., Dong, S., Hou, Y., Xu, H., Gu, W., Li, Q., & Zhao, X. 2024. Numerical modelling of the spatial distribution of wave overtopping water behind dikes under regular wave action using OpenFOAM. *Ocean Engineering*, *309*, 118551. https://doi.org/10.1016/j.oceaneng.2024.118551